Fricke-Xylenol orange-Gelatin gel characterization with dual wavelength cone-beam optical CT scanner for applications in stereotactic and dynamic radiotherapy

Alice Rousseau, Christel Stien, jean-marc bordy, Valentin Blideanu

Title:

Fricke-Xylenol orange-Gelatin gel characterization with dual wavelength cone-beam optical CT scanner for applications in stereotactic and dynamic radiotherapy

Author names and affiliations:
Alice Rousseau[a] (corresponding author) ; alice.rousseau@cea.fr
Christel Stien[a] ; christel.stien@cea.fr
Jean-Marc Bordy[a] ; jean-marc.bordy@cea.fr
Valentin Blideanu[a] ; valentin.blideanu@cea.fr

[a]Université Paris-Saclay, CEA, List, Laboratoire National Henri Becquerel (LNE-LNHB), F-91120 Palaiseau, France.

Declarations of interest: none.

Abstract:
Purpose: This study is about the development of a new dual wavelength reading method of Fricke-Xylenol orange-Gelatin (FXG) gel dosimeters on the Vista16™ optical Computed Tomography (CT) scanner to perform 3D dose distribution measurements in stereotactic and dynamic radiotherapy treatments.
Methods: The dosimetric characteristics of an optimized FXG gel composition and its optical CT readout have been evaluated. A dual wavelength reading method has been developed on the CT scanner at wavelengths 590 nm and 633 nm. Small-field dose profile measurements with FXG gel and microDiamond (PTW) detectors were compared by γ-index analysis (0.5%/0.5mm) to validate this method.
Results: This reading method exhibits linear calibration curves in the 0 – 4 Gy and 2 – 10 Gy dose ranges at 590 nm and 633 nm respectively. The absorbed dose values below 4 Gy, measured at 590 nm, and those above 4 Gy, measured at 633 nm, are combined to plot a complete profile. A γ passing rate of 93.4 % was achieved.
Conclusions: The new reading method of FXG gel dosimeters has been implemented on the Vista16™ scanner to span absorbed doses representative of stereotactic and dynamic radiotherapy treatments and enable 3D measurements in tumor volumes and surrounding healthy tissues. Small-field profile measurements validated this reading method as FXG gel dosimeters and microDiamond detectors were in very close agreement. This dosimetric method is a promising candidate for 3D quality assurance end-to-end tests in stereotactic and dynamic radiotherapy.

Keywords:
Fricke-based gel dosimetry, optical CT scanner, stereotactic radiotherapy, 3D dosimetry

1. Introduction

In external radiotherapy, complex and sophisticated treatment techniques such as Intensity-Modulated Radiation Therapy (IMRT) and stereotactic radiotherapy are becoming widely used in clinics. These techniques are designed to fit tightly the target volumes and deliver complex and non-uniform dose distributions with steep dose gradients. However, the dosimeters currently available in clinics only measure point or planar dose distributions, or can be assembled in 2D or 3D arrays to provide 2D or sparse 3D dose distributions with a low spatial resolution.

Gel dosimetry is therefore a promising candidate to provide 3D dose distributions [1–3]. Gel dosimeters undergo chemical changes upon irradiation that are spatially fixed in a 3D matrix. They present great potential to perform end-to-end quality assurance, as they can represent the tumor volume and surrounding tissues and can be designed to fit into cavities in commercial anthropomorphic phantoms [4].

Fricke gel dosimeters were the first to be studied [5]. Their components are ultra-pure deionized water, a ferrous ammonium sulfate solution, sulfuric acid and a gelling agent (gelatin, agarose or polyvinyl alcohol [6]). The radiation-induced changes consist in the ferrous ions (Fe^{2+}) being oxidized into ferric ones (Fe^{3+}). Fricke gel dosimeters are tissue equivalent over the range of megavoltage (MV) photon energies [2]. However, they do not retain a spatially stable dose distribution after irradiation due to ferric ion diffusion in the gel matrix. Imaging of the dosimeter must then be performed on time scales of 1 to 2 hours [6]. Yet chelating agents can be added to the gel formulation to reduce ion diffusion [7].

Gel dosimeters can be read using a Magnetic Resonance Imaging (MRI) or an optical Computed Tomography (CT) readout [5,8]. The color change occurring in radiochromic gel dosimeters, such as Fricke-based gel dosimeters containing a chelating agent, enables the measurement of 3D maps of optical attenuation with optical CT scanners. Cone-beam optical CT scanners are based on a converging light source and a CCD camera. They scan samples in about 5 minutes [3], are compact and not expensive. ModusQA (London, Ontario, Canada) commercializes cone-beam CT scanners under the name Vista™.

Fricke-Xylenol orange-Gelatin (FXG) gel dosimeters combined to an optical readout were introduced in 2000 [9]. They consist in a Fricke-based gel with a matrix of gelatin into which a chelating agent, the xylenol orange (XO), is added. The ferrous ions oxidized into ferric ions after irradiation bond to the molecules of the XO to form the XO-Fe(III) complex. This complex absorbs around 585 nm and makes the colour of the gel going from yellow to purple-brown. The composition of the FXG dosimeters was investigated and optimized in previous papers [9–11] in terms of sensitivity, post-irradiation stability, absorbed dose range, etc. The authors used concentration values of 3 to 6 %wt of gelatin, 0.3 to 1.0 mM of ferrous ammonium sulfate, 50 or 65 mM of sulfuric acid and 0.05 to 0.15 mM of XO.

Optical CT scanners have already been used to measure 3D dose maps with FXG gel dosimeters. Babic *et al* 2008 [3] inserted a FXG gel cylinder in a head-and-neck phantom to develop a 3D IMRT dose verification protocol. A comparison was made between the treatment plan and the measurements performed by gel dosimetry with optical CT readout. However, the dose normalization point of the treatment plan had to be rescaled for gel dosimetry (from 6.8 Gy to 2.0 Gy) to avoid optical saturation during the readout. In Ramm 2018 [12], a fluid-less dual wavelength optical CT scanner was developed to provide an alternative time-sparing reference scan to the commonly used pre-irradiation scan. It was based on the simultaneous scanning of an irradiated gel dosimeter at two wavelengths, with the gel dosimeter displaying a reduced dose response at the second wavelength so that this scan could replace the pre-irradiation scan. This scanner was used to perform small-field measurements with maximum doses ranging from 3 to 4 Gy with FXG gel dosimeters. As shown in these papers, it is already feasible to measure 3D dose distributions by FXG

gel dosimetry associated to an optical CT readout. However, the dose range measured with such methods is not representative of stereotactic and dynamic treatment techniques that can easily reach 10 Gy.

In this paper, a FXG gel associated to a cone-beam optical CT scanner readout (Vista16™) was investigated to be used for applications in dynamic and stereotactic treatment techniques. This dosimetric method was developed to provide a linear dose response over a dose range clinically representative, measuring small out-of-field doses and high doses delivered to the tumor volumes. For this purpose, a FXG gel composition was first optimized by spectrophotometric analysis. A new dual wavelength reading method of the FXG gel dosimeters was then developed on the Vista16™ scanner at wavelengths 590 nm and 633 nm to span an absorbed dose range up to 10 Gy. This dosimetric method was characterized in terms of chemical reaction time, ferric ion diffusion, dose resolution, threshold dose and dose rate and energy dependencies. It was then validated by performing small-field profile measurements with FXG gel and microDiamond (PTW) detectors, and comparing them with a γ-analysis of 0.5 % dose difference and 0.5 mm distance-to-agreement passing criteria.

2. Materials and methods

2.1. FXG gel preparation

The FXG gel constituents are ultrapure deionized water (MilliQ, Millipore), gelatin from porcine skin of gel strength 300, Type A (Sigma-Aldrich, G2500-1KG), ferrous ammonium sulfate (Fluka, 09719-50G), sulfuric acid (Fluka, 84716-1L) and XO (Acros Organics, 211220050). Gelatin is dissolved into MilliQ water at approximately 45°C. Once the dissolution is complete, the solution is acidized by adding sulfuric acid until the pH intended for the experiment is reached. Ferrous ammonium sulfate and XO are then successively dissolved in the solution. The homogeneity of the mixture is obtained by stirring it during the whole process, maintaining the temperature of the solution around 45°C. The solution is then poured into the dedicated containers, which are (Fig. 1):

i) PMMA cuvettes of 1 cm path length for spectrophotometric measurements,

ii) Teflon-FEP cylinders of 3.9 cm diameter and 6.3 cm height for optical CT readout.

Once filled, the containers are closed without leaving air bubbles and left to cool at room temperature for 15 minutes. They are then stored in a 6°C refrigerator for at least 4 hours. The gel dosimeters are prepared one day before their irradiation and are placed in the irradiation room a few hours before being irradiated for thermal stabilization. One batch of gel is prepared for each experiment.

2.2. Irradiations

Gel irradiations were carried out in the primary beams of the French national metrological laboratory for ionizing radiation, the Laboratoire National Henri Becquerel (LNHB) at CEA List. They were performed following the TRS 398 recommendations for absorbed dose to water irradiations in reference conditions (10 x 10 cm^2 field size, Source to Surface Distance SSD = 90 cm and the center of the gel dosimeter placed at the reference depth of 10 cm into water). A 30 x 30 x 30 cm^3 water phantom, a dose rate of 400 MU/min and 6 MV WFF (With Flattening Filters) photon beams were used on a Truebeam (Varian Medical Systems, Palo Alto, CA) linear accelerator unless otherwise indicated. Irradiations of the dosimeters were performed in the 0.05 – 22 Gy absorbed dose range.

2.3. Optimization of the FXG gel composition

The FXG gel composition was optimized to be used in stereotactic and dynamic radiotherapy treatments as a dosimeter for 3D quality assurance (QA). The aim was to find the most sensitive gel

composition with a linear dose response on a dose range corresponding to the clinical one. The sensitivity of the gel was defined as the slope of its linear dose response curve over the dose range studied. This optimization was performed with the UV-Vis Cintra 4040 spectrophotometer (GBC Scientific) to get quick and precise point measurements. Optical readout of the cuvettes was conducted at 590 nm, which corresponds to a wavelength close to the absorption peak of the XO-Fe(III) complex. Optical attenuation coefficients $\Delta\mu$ (in cm^{-1}) were calculated from spectrophotometric measurements with the expression:

$$\Delta\mu = \frac{\Delta A * ln(10)}{l} \quad (1)$$

where ΔA is obtained by subtracting the absorbance measured on a non-irradiated cuvette to the one measured on the irradiated one and $l = 1$ cm is the path length of the cuvettes. Ten absorbance values for each cuvette were measured and averaged. Error bars correspond to the standard deviations of the mean optical attenuation coefficients.

The influence of each constituent in the gel composition was studied for different concentrations, while keeping all other constituents at a constant concentration. The concentrations of the gel components and the pH of the gel for each experiment can be found in Table 1, as well as the number of different FXG gel batches used for each experiment. The results obtained enabled to find the optimal concentrations of the components of the gel and its optimal pH. This optimized FXG gel composition was then used for this study.

2.4. Optical CT readout

Once the FXG gel composition was optimized, the next step was to scan gel dosimeters with a cone-beam optical CT scanner to obtain 3D spatial dose information. The outer dimensions of the cylindrical dosimeters have been selected to fit the dimensions of the commercial anthropomorphic phantom inserts available for stereotactic and dynamic treatments 3D QA, e.g. between 3 cm and 5 cm diameter.

The cone-beam optical CT scanner Vista16™ (ModusQA) was used for the optical readout of the Teflon-FEP gel cylinders. Two LED light sources of wavelengths 590 nm and 633 nm were used in this work for the readings of the gels. A reference scan of the dosimeter before its irradiation and a data scan post-irradiation of each 2000 projections were acquired at both wavelengths. The Feldkamp-Davis-Kress (FDK) algorithm and a Hamming filter were applied for the reconstruction with voxels of dimensions 0.5 x 0.5 x 0.5 mm^3 [13]. The matching liquid in the tank was a mixture of 10 %wt propylene glycol – deionized water for a better refractive index match between FXG gel, Teflon-FEP material and matching liquid. The scanner was always switched on two hours before use to reach thermal stabilization [14].

2.5. FXG gel – optical CT readout characterization

2.5.1. Chemical reaction time

The time required for the radio-induced chemical reactions occurring in the gel before reaching completion has been evaluated in order to scan the gel dosimeters only when their responses are stable in time. Cuvettes irradiated at 2 Gy, 5 Gy and 10 Gy were read repeatedly at 22°C during two hours by spectrophotometry at 590 nm. The absorbance measured on a non-irradiated cuvette was systematically subtracted, as we made the assumption that the spontaneous oxidation of Fe^{2+} ions would occur at a similar rate for irradiated and non-irradiated cuvettes.

2.5.2. Diffusion coefficient calculation

Radio-induced chemical reactions occurring in the FXG gel generate ferric ions that diffuse in the gel matrix. This phenomenon can be characterized by the ferric ion diffusion coefficient d (m^2 s^{-1}). The

method used in this work to determine this coefficient is based on the Fick's second law and on the measurements performed with MRI readings in Coulaud *et al* 2019 [15].

The experiment consisted in placing a cylindrical gel dosimeter in a water tank with its rotation axis perpendicular to the beam axis. The center of the cylinder was put at the reference depth into the tank and at one of the edges of the irradiation beam (Fig. 2). The gel dosimeter was irradiated on one half at 5 Gy at reference point.

The gel flask was then scanned repeatedly over time at 22°C by CT scanner at 633 nm. The optical attenuation coefficient $\Delta\mu(x,t)$ can be related to the Fe^{3+} ion concentration with a complementary error function [15]:

$$\Delta\mu(x,t) = \frac{\Delta\mu_{irr} - \Delta\mu_0}{2} * Erfc\left(\frac{x - x_0}{2\sqrt{d * t}}\right) + \Delta\mu_0 \quad (2)$$

where $\Delta\mu_0$ (cm^{-1}) is the attenuation coefficient of the non-irradiated part of the gel, $\Delta\mu_{irr}$ (cm^{-1}) is the attenuation coefficient of a homogeneous distribution of Fe^{3+} ions in the irradiated part of the gel (before the diffusion has begun), and x_0 (cm) is the coordinate at the center of the interface between irradiated and non-irradiated gel regions . A Levenberg-Marquardt algorithm was used to fit the optical attenuation profiles acquired at different times during six hours. This way, the standard deviation σ (m^2) of the complementary error function was calculated for each profile. Assuming that the FWHM (Full Width at Half Maximum) of the Gaussian function in the solution of the Fick's second law and the one of the complementary error function are related equally to the diffusion coefficient [7], the following relation was obtained:

$$\frac{\sigma^2}{2} = d * t \quad (3)$$

so that, by plotting $\frac{\sigma^2}{2} = f(t)$, the diffusion coefficient d of the Fe^{3+} ions in the FXG gel was measured. 80%-20% penumbra widths were also measured for each profile to evaluate the difference of penumbra width with time compared to an ideal non-diffusing profile extrapolated at time $t = 0$.

2.5.3. Dose resolution

The concept of dose resolution D_Δ^p represents the minimal separation between two absorbed doses such that they may be distinguished with a given level of confidence p. The expression of the dose resolution for a 95% level of confidence is [16]:

$$D_\Delta^{95\%} = 2{,}77 * u_c(D) \quad (4)$$

where $u_c(D)$ is the combined uncertainty on the absorbed dose D. For this experiment, the 590 nm and 633 nm light sources were used. A cylindrical gel dosimeter was successively irradiated to doses between 0.25 Gy and 5 Gy for the 590 nm reading, and another one between 0.25 Gy and 10 Gy for the 633 nm reading. For each dose, a mean optical attenuation coefficient $\Delta\mu$ was obtained by averaging the voxel values contained in a cylindrical region of interest (ROI) of radius 5 mm and height 10 mm located at the center of the gel cylinder. We considered here that the FXG gel read by optical CT scanner presented a polynomial dose response as the dose ranges investigated for each wavelength were larger than those where the gel displayed a linear response:

$$D = a * \Delta\mu^2 + b * \Delta\mu + c \quad (5)$$

where a (Gy cm^2), b (Gy cm) and c (Gy) correspond to the fit parameters. Therefore, $u_c(D)$ can be calculated with the law of propagation of uncertainties:

$$u_c^2(D) = \left(\frac{\partial D}{\partial a}\right)^2 * u^2(a) + \left(\frac{\partial D}{\partial b}\right)^2 * u^2(b) + \left(\frac{\partial D}{\partial c}\right)^2 * u^2(c) + \left(\frac{\partial D}{\partial \Delta\mu}\right)^2 * u^2(\Delta\mu) + 2\left[\frac{\partial D}{\partial a} * \frac{\partial D}{\partial b} * u(a,b) + \frac{\partial D}{\partial a} * \frac{\partial D}{\partial c} * u(a,c) + \frac{\partial D}{\partial b} * \frac{\partial D}{\partial c} * u(b,c)\right] \quad (6)$$

where $u(a)$, $u(b)$, $u(c)$ and $u(\Delta\mu)$ are the standard uncertainties of a, b, c and $\Delta\mu$ respectively, and $u(a,b)$, $u(a,c)$ and $u(b,c)$ are the covariant terms. The standard deviation of the distribution of the voxels in each ROI was considered equal to the uncertainty associated to the mean optical attenuation, $s(\Delta\mu)_{exp} = u(\Delta\mu)$. Equation (6) can be simplified:

$$u_c^2(D) = \Delta\mu^4 * u^2(a) + \Delta\mu^2 * u^2(b) + u^2(c) + (2 * a * \Delta\mu + b)^2 * u^2(\Delta\mu) + 2 * \Delta\mu[\Delta\mu^2 * u(a,b) + \Delta\mu * u(a,c) + u(b,c)] \quad (7)$$

Using the combined uncertainty on the absorbed dose ($u_c(D)$) in the calculation of $D_{\Delta}^{95\%}$ rather than just the standard deviation $s(\Delta\mu)_{exp}$ took into account the goodness of the fit applied to the experimental data [17]. The relative dose resolution was finally defined as [18]:

$$D_{\Delta,\%}^{95\%} = \frac{D_{\Delta}^{95\%}}{D} \quad (8)$$

2.5.4. Threshold dose

Some papers reported an apparent threshold dose when using FXG gel dosimeters scanned optically around 590 nm [12,19]. An experiment was therefore conducted to verify if a threshold dose was noticeable for the FXG gel composition presented in this study. Twelve gel cylinders were exposed to doses between 0.05 Gy and 3 Gy and were read 20 min post-irradiation at 590 nm by optical CT scanner.

2.5.5. Dose rate and energy dependencies

To evaluate the dose rate and energy dependencies of the FXG gel, two experiments were performed using cuvettes filled with gel. Ten cuvettes were exposed to 5 Gy per dose rate (at 6 MV WFF photon energy) for dose rates between 100 MU/min and 600 MU/min, or per photon energy (at 400 MU/min) for 6, 10, 15 and 20 MV WFF. The cuvettes were then scanned by spectrophotometry at 590 nm. In each experiment, a mean optical attenuation coefficient $\overline{\Delta\mu}$ was calculated for the 10 cuvettes. The dosimeter sensitivity for each dose rate or each quality index ($TPR_{20,10}$) was defined as:

$$s = \frac{\overline{\Delta\mu}}{D} \ (\mathrm{cm}^{-1}\ \mathrm{Gy}^{-1}) \quad (9)$$

with the uncertainty

$$u(s) = \sqrt{(\frac{\partial s}{\partial \overline{\Delta\mu}})^2 * u(\overline{\Delta\mu})^2 + (\frac{\partial s}{\partial D})^2 * u(D)^2} = \sqrt{\frac{1}{D^2} * u(\overline{\Delta\mu})^2 + \frac{\overline{\Delta\mu}^2}{D^4} * u(D)^2} \quad (10)$$

where $u(\overline{\Delta\mu})$ is the standard deviation of the mean optical attenuation and $u(D)$ the uncertainty on the absorbed dose.

With another batch of gel, the dose rate dependency study was also performed with a 6 MV FFF (Flattening Filter Free) beam with dose rates between 600 MU/min and 1400 MU/min. Sensitivities were then compared for 6 MV photon beams with and without flattening filters.

2.6. Implementation of a dual wavelength reading method

2.6.1. Small-field dose profile measurements

Small-field dose profile measurements were performed by FXG gel dosimetry combined to an optical CT readout and with the PTW 60019 microDiamond detector. This diamond detector presents a sensitive volume of 0.004 mm^3, a radius of 1.1 mm and a thickness of 1 µm. It was placed in the water tank with its revolution axis being parallel to the beam axis for the measurements. A scanning step of 0.5 mm was used. The diamond detector was considered as our 'gold standard' detector for small-field 2D measurements upon which gel measurements were compared. The 80%-20%

penumbra widths of each profile and their FWHM were calculated. A global γ-index analysis with passing criteria 0.5 % dose difference and 0.5 mm distance-to-agreement was performed.

2.6.2. Dual wavelength reading method: implementation and validation

The comparison between gel and diamond measurements is a test case to validate the new dual wavelength reading method of FXG gel dosimeters proposed in this study for extending the dose range of its applicability.

Two experiments were performed on different days with FXG gel dosimetry. A same batch of gel was used for a whole experiment. Linear calibration curves $D = a_\lambda * \Delta\mu + b_\lambda$ ($\lambda = 590$ nm or 633 nm) were established at both wavelengths (see Discussion) for the 6 MV photon beam (WFF or FFF) considered in the experiment. They were obtained by irradiating several gel cylinders at known doses on the 0.25 – 4 Gy dose range for the 590 nm scanning and on the 2 – 10 Gy dose range for the 633 nm one. The coefficients $\Delta\mu$ in the expression are the average values measured within the voxels contained in the cylindrical ROIs of the gel vials (as described in Section 2.5.3).

In each experiment, a FXG gel cylinder was irradiated in a water phantom at reference depth either at i) 8.9 Gy with a 6 MV WFF beam of field size 2 x 2 cm^2 or at ii) 8.6 Gy with a 6 MV FFF beam of field size 1 x 1 cm^2. These dosimeters were first optically scanned 20 min post-irradiation at 590 nm, to obtain a stable response in time (see Section 3.3.1), and then 45 min post-irradiation at 633 nm. After the reading at 590 nm, the 633 nm light source was placed onto the scanner benchtop. Before using this light source, it was switched on at least two hours on an external power supply and then switched off for only 2 min maximum for mounting. A thermal stabilization time of 20 min was needed in this configuration. Therefore, the heating time of the scanner for the second reading was low enough to limit the diffusion effects (see Discussion), as the total measurement time (including readings at 590 nm and 633 nm that last 5 min each) was 50 min.

Dose profiles were finally obtained by combining the dose values below 4 Gy measured at 590 nm and those above 4 Gy measured at 633 nm (the choice of the 4 Gy threshold value is explained in the Discussion). FXG gel flasks were all stored more than 8 hours at room temperature before irradiation to negate an apparent threshold dose at low doses (see Discussion).

2.7. Uncertainty budget

The dose rate and energy dependencies of the FXG gel were considered as negligible (Discussion section). As the gel flasks were stored under the same temperature conditions as the irradiation room a few hours before irradiation, we considered the influence of the temperature of irradiation as negligible.

For every gel flask used to establish the calibration curves at 590 nm and 633 nm, the standard uncertainty on the dose D delivered under the TRS 398 reference conditions with the Truebeam accelerator, $u(D)_{stand}$, was given by 0.47 %. The combined uncertainty on the optical attenuation took into account the uncertainties associated to the flask repositioning between the acquisition of the reference and data scans, the ROI at the center of each calibration flask for $\Delta\mu$ determination, a reading temperature variation of ± 0.1°C and a post-irradiation waiting time between 20 min and 50 min. As the spontaneous oxidation was found linear with time and reproducible for non-irradiated gel flasks of a same batch, a correction of this effect was applied to the data. It consisted in subtracting the mean optical attenuation coefficient of a ROI at the center of an unirradiated flask to the optical attenuation coefficients of the irradiated flasks corresponding to the time between the acquisition of the reference and data scans of each irradiated flask.

Based on these uncertainties, the linear fits, applied to the data to establish the calibration curves, provided the uncertainties associated to the fit parameters, a_λ and b_λ. As for the calibration flasks, the combined uncertainty on the optical attenuation coefficients along the profile measurements

took into account the uncertainties associated to the flask repositioning, the correction for spontaneous oxidation, the reading temperature variation and the post-irradiation waiting time. As explained in Section 2.6.2, the uncertainties associated to the diffusion effects could be neglected. The flasks irradiated to perform the profile measurements were always from the same gel batch than the calibration flasks, which led us not to consider an inter-batch reproducibility. Finally, we considered that the intra-batch reproducibility was taken into account in the dispersion of the data along the calibration curve as long as at least eight gel flasks were used to establish the calibration curve. An uncertainty budget that lists the sources of uncertainty to determine the combined uncertainty on $\Delta\mu$ coefficients can be found in Table 2. All reported uncertainties are at k=1.

3. Results:

3.1. Optimization of the FXG gel composition

The dose response curves for each batch of gel prepared with different pH are shown in Fig. 3 (a). The gel was sensitive for pH values between 1.0 and 2.5. However, the highest sensitivities on the largest dose range (1 – 6 Gy) were found for pH between 1.5 and 1.9 (7.0 % maximum difference between the slopes within this pH range, see Fig. 3 (b)). For pH > 3.0, spontaneous oxidation of Fe^{2+} ions already occurred since the gel batches were violet without radiation exposure. On the other hand, for low pH values (< 1.5), XO-Fe(III) complexes could be dissociated and H^+ ions preferably bond with XO molecules instead of Fe^{3+} ions [19].

Linear regressions on the absorbed dose range up to 6 Gy for 4 %wt to 6 %wt gelatin concentrations displayed sensitivities and initial absorbance values (of the non-irradiated cuvettes) listed in Table 3. The sensitivities did not significantly change with gelatin concentration. However, initial absorbance values increased with gelatin concentration, inducing less transparency of the gel. As a compromise between an increased transparency and a reduced ferric ion diffusion (conditioned by a high gelatin concentration [15]), we selected a 5 %wt gelatin concentration.

Fig. 4 (a) displays the gel dose responses for different XO concentrations (from 0.04 mM to 0.13 mM). The response of the gel was linear on a wider dose range when increasing XO concentration (D_{max} values in Fig. 4 (b)). However, a diminution of the gel sensitivity was observed with higher XO concentrations (Fig. 4 (b)). A XO concentration of 0.09 mM was thus selected to provide a linear dose response with the best achievable sensitivity for irradiations up to 10 Gy, as this dose range is representative of stereotactic and dynamic radiotherapy.

The influence of the Fe^{2+} ion concentration on the dose response curves of the gel is represented in Fig. 5 (a). The linear dose response range was similar for the four concentrations (2 – 14 Gy). The sensitivities on this dose range (Fig. 5 (b)) did not enlighten any impact of Fe^{2+} ion concentration on the sensitivity of the gel. However, as the natural oxidation rate of Fe^{2+} ions is proportional to the square of Fe^{2+} ion concentration in the gel composition, resulting in a reduced stability of the gel dosimeter in time [10], a concentration of 0.3 mM was chosen.

The final FXG gel composition was selected as a 5 %wt of gelatin, a pH of 1.6, a 0.3 mM of ferrous ammonium sulfate and a 0.09 mM of XO. Compared to stereotactic and dynamic applications involving FXG gels and optical CT readout in the literature [3,12], the XO concentration selected in this study is the main parameter that has been modified.

3.2. Optical CT readout: second reading wavelength

When cylindrical gel flasks were scanned at 590 nm, it was found that the gel became too dark to be read correctly at this wavelength when it had been exposed to more than 5 Gy, as the contrast difference between the gel and the matching liquid surrounding it during the reading was too important. Therefore, a 633 nm reading was implemented on the CT scanner to read higher doses. As

the optical absorption of the gel is lower at this wavelength than at 590 nm (see Fig. 6), the contrast difference is less important at 633 nm.

3.3. FXG gel – optical CT readout characterization

3.3.1. Chemical reaction time

Fig. 7 displays the optical attenuation measured repeatedly for two hours between the gel cuvettes exposed to 2 Gy, 5 Gy and 10 Gy and a non-irradiated cuvette. The attenuation increased quickly up to 20 minutes after irradiation for the three doses, and then seemed to be stable to at least 2 hours. Within the time interval between 20 minutes and 120 minutes, attenuation increases by about 1 % h^{-1} were measured for the 2 Gy and 5 Gy exposures. No increase was detected at 10 Gy. The increase of attenuation at 2 Gy and 5 Gy could come from two sources: minor radio-induced chemical reactions still occurred after 20 min post-irradiation, and the spontaneous oxidation rate was in fact not strictly the same for an irradiated cuvette and a non-irradiated one. In any case, a post-irradiation waiting time before imaging selected between 20 min and 2 h limits to 1.0 % h^{-1} the optical attenuation variation for doses up to 10 Gy.

3.3.2. Diffusion coefficient calculation

Fig. 8 (a) displays the evolution over time of the profiles measured after irradiation. For the sake of clarity, only three profiles are represented instead of the 12 that were acquired during six hours. As expected, the penumbra width of the profile increased with time due to the diffusion of the ferric ions from the irradiated part of the gel (< 2.4 cm) to the non-irradiated one (> 2.4 cm). The effect of spontaneous oxidation of Fe^{2+} ions was observed in the two plateaus of the irradiated and non-irradiated gel regions as their respective optical attenuation increased with time. Spontaneous oxidation rates of 0.0030 cm^{-1} h^{-1} and 0.0018 cm^{-1} h^{-1} have been measured for the irradiated and non-irradiated gel parts respectively, indicating that spontaneous oxidation did not present the same rate for irradiated and non-irradiated gel parts.

For each profile, the σ^2 value of the complementary error function was calculated. The curve $\frac{\sigma^2}{2} = f(t)$ is plotted in Fig. 8 (b). The slope of the linear regression corresponds to the ferric ion diffusion coefficient in the FXG gel and is equal to $d = 2.46 \pm 0.04\ 10^{-10}\ \mathrm{m^2\ s^{-1}}$.

80%-20% penumbra widths were finally measured for each profile and plotted versus time after irradiation. A linear regression allowed us to calculate the initial penumbra width (as the chemical reactions lasted 20 minutes after irradiation, the ideal non-diffusing profile could only be virtual with FXG gel dosimetry), $(80\% - 20\%)_0 = 4.9$ mm. From that equation, we could also deduce the difference of penumbra width between the initial profile and the one measured with gel dosimetry at a given time.

3.3.3. Dose resolution

Fig. 9 (a) and (b) display the FXG gel dose response on the 0.25 – 5 Gy dose range at 590 nm and the 0.25 – 10 Gy dose range at 633 nm. From these graphs, it was found that the FXG gel response was linear from 0.5 Gy to 4 Gy when scanned at 590 nm and from 2 Gy to 10 Gy at 633 nm. The dose resolution $D_{\Delta}^{95\%}$ and the relative dose resolution $D_{\Delta,\%}^{95\%}$ are plotted in Fig. 9 (c) and (d). For the 590 nm reading, even though dose resolutions obtained below 1 Gy are among the lowest ones, they are high considering the relative dose resolution values associated (> 7.7%). On the other hand, on the 1 – 4 Gy dose range, the relative dose resolution is low (between 3.6 % and 5.6 %), while the absolute value keeps increasing. Therefore, the best dose resolution values associated to small relative dose resolution values were found for dose values between 1 Gy and 2 Gy. They are between 0.056 Gy and 0.077 Gy (see Table 4).

On the 2 – 10 Gy dose range at the 633 nm reading, the relative dose resolution kept decreasing (from 14.0 % to 4.3 %) while the dose resolution was increasing (passing from 0.28 Gy to 0.43 Gy).

The best dose resolution values were obtained in the 6 – 10 Gy dose range (between 0.32 Gy and 0.43 Gy) when small dose resolution values were associated (between 4.3 % and 5.4 %), as reported in Table 4.

3.3.4. Threshold dose

When investigating the FXG gel dose response at low doses, between 0.05 Gy and 3 Gy, two different linear regimes were found (Fig. 10). The first one was below 0.5 Gy and the second above 0.5 Gy, with a slope higher for doses below 0.5 Gy. Focusing on the 0.5 – 3 Gy dose range leads to an apparent threshold dose of 0.09 ± 0.03 Gy. However, we found here that this threshold was only virtual, as doses as low as 0.05 Gy could actually be measured.

3.3.5. Dose rate and energy dependencies

The gel dosimeter sensitivities obtained by exposing gel cuvettes to 5 Gy for each dose rate and each quality index ($TPR_{20,10}$) are represented in Fig. 11. No trend in sensitivity with dose rate or with quality index was observed.

3.4. Dual wavelength reading method and small-field dose profile measurements

Fig. 12 (a) and (c) display the 2 x 2 cm^2 6 MV WFF and 1 x 1 cm^2 6 MV FFF dose profiles obtained with the 590 nm and 633 nm readings of two gel dosimeters exposed to 8.9 ± 0.1 Gy and 8.6 ± 0.1 Gy respectively (circles and triangles are the experimental values, lines are displayed to guide the eye). It can be noticed that, above 5.5 Gy approximately, the 590 nm reading presented biased dose values as the CCD camera saturated for the optical attenuation coefficients corresponding to that dose range. Below 2 Gy, a difference could also be perceived between the two profiles, with dose values obtained at 633 nm that are overestimated compared to those at 590 nm.

A combined dose profile was defined for each experiment using the dual wavelength reading method with the dose values obtained at 590 nm below 4 Gy and those obtained at 633 nm above 4 Gy. A cubic spline interpolation of these data points was applied [20]. After that, relative dose profiles were obtained with normalization at the maximum dose value. These profiles were then compared to the relative ones acquired with the diamond detector (Fig. 12 (b) and (d)). γ indices with passing criteria 0.5%/0.5mm are reported in the same figure (green and red stars). Only four points exceed the criteria in the two figures. FWHM, 80%-20% penumbra widths and γ passing rates for the gel and diamond profiles can be found in Table 5. There is only a difference of 0.2 mm between the FWHM measured with the two dosimeters and of 0.4 mm and 0.5 mm for the penumbra widths. These differences are consistent with the 0.5 mm spatial resolution of the profile measurements of the two dosimeters. A very good γ passing rate of 93.4 % for the two profiles was found considering the strict criteria 0.5%/0.5mm.

4. Discussion:

The first part of this study consisted in optimizing the FXG gel composition by spectrophotometric analysis for applications in stereotactic and dynamic treatment techniques. The final composition is the following: 5 %wt gelatin concentration, pH of 1.6, 0.3 mM ferrous ammonium sulfate and 0.09 mM XO. This composition presents a linear response as sensitive as possible up to 10 Gy. Compared to the literature [3,12], it allows to measure doses higher than 4 Gy, meaning it could be used for dose measurements inside the target of an actual treatment plan.

Dosimetric performances of the FXG gel and the Vista16™ scanner were investigated to evaluate the interest of this method for stereotactic and dynamic applications. We did not observe any dose rate dependency (between 100 MU/min and 600 MU/min) or energy dependency (between 6 MV and 20

MV WFF high energy photon beams) for the FXG gel presented here, within the limits of the uncertainties. The same conclusions for dose rate dependency were made for a 6 MV FFF beam (between 600 MU/min and 1400 MU/min), as well as the comparison between 6 MV WFF and FFF beams.

The ferric ion diffusion coefficient $d = 2.46 \pm 0.04\ 10^{-10}\ \mathrm{m^2\ s^{-1}}$ was determined for our FXG gel composition. Two ferric ion diffusion coefficients of FXG gel dosimeters with similar compositions and optical readings have been reported in the literature (Table 6) [21,22]. The method of determination of the diffusion coefficient based on a complementary error function is used in this study and in Oliveira *et al* 2014 [22], whereas Solc *et* Spevacek 2009 [21] used an inverse square root function. The fitting of the data in the gradients of the profiles is of the same quality for these two methods. Therefore, the two functions are expected to give similar results in the determination of the ferric ion diffusion coefficient.

However, the diffusion coefficients reported in these two papers are slightly smaller than the one measured in this study. Gelatin concentrations are the same in these three gel compositions, but we use a lower XO concentration (of 0.09 mM vs 0.1 mM in the other two papers). As it has been reported that the concentrations of these constituents highly influence the ferric ion diffusion occurring in the gel matrix [7,15], that could explain those differences. Nevertheless, we can still consider that these three diffusion coefficients are close enough, around $2.0 - 2.5\ 10^{-10}\ \mathrm{m^2\ s^{-1}}$, given the fact that they were not determined at the same temperature.

We also found that the diffusion effects occurring in the gel dosimeter cause an increase of at least 0.5 mm of the 80%-20% penumbra width in a profile measurement at a reading time above 50 min, compared to the initial one at time $t = 0$. As the voxels in the 3D distributions present a spatial resolution of 0.5 mm, a reading time $t > 50$ min will induce a spatial deformation of the dose distribution noticeable with this readout technique. Therefore, the ideal reading time of the FXG gel dosimeter is between 20 min, in order to reach chemical reaction completion, and 50 min after irradiation.

In order to set up the dual wavelength reading method, dose resolutions were used as criterion for determining the dose range of use of both wavelengths. Dose resolutions between 0.056 Gy and 0.15 Gy were measured at 590 nm for the 0.5 – 4 Gy dose range. These values are much smaller than the ones measured at 633 nm, which are between 0.28 Gy and 0.43 Gy for the 2 – 10 Gy dose range. In fact, the dose resolutions at 590 nm are at least two times smaller than the ones found in the literature, where dose resolution values are between 0.2 Gy and 0.9 Gy for doses up to 10 Gy and for different types of gels and reading methods (see Table 7) [23–25]. On the other hand, the dose resolutions measured at 633 nm are of the same order than the ones reported in the literature. However, it is important to notice that the dose ranges spanned at each wavelength for a linear response of the gel are different (0.5 – 4 Gy at 590 nm, 2 – 10 Gy at 633 nm). This is due to the early saturation in optical attenuation of the CCD camera when performing the optical reading at 590 nm and to a reduced sensitivity of the gel when scanned at 633 nm (Fig. 6).

A dual wavelength reading method was therefore developed on the CT scanner to scan FXG gel dosimeters at 590 nm for low doses (inferior to 4 Gy) and at 633 nm for high doses (on the 4 – 10 Gy dose range), see Fig. 12 (a) and (c). A threshold value of 4 Gy was selected to have the most sensitive FXG gel response up to 4 Gy with the 590 nm reading, before switching to 633 nm. A second reading wavelength had never been used before to scan FXG gel dosimeters in order to extend the dose range of use.

An apparent threshold dose of 0.09 ± 0.03 Gy was measured at 590 nm on the CT scanner. This threshold dose is close to the one measured in Babic *et al* 2008 [19] of 0.20 ± 0.05 Gy for a close FXG gel composition with a spectrophotometric readout at 594 nm. As two linear regimes of different slopes were found in our study on the 0.05 – 3 Gy dose range with a delimitation at 0.5 Gy (Fig. 10), it

is preferable to work in the linear regime above 0.5 Gy. Two options could therefore be followed as suggested in [19]. Gel cylinders could receive a uniform 'priming' dose of 0.5 Gy, but that would require supplementary irradiations that are time-consuming and the uniformity is not easily obtained in 3D volumes. The other option is the one adopted here. It consists in increasing the Fe^{3+} ion concentration through spontaneous oxidation of the Fe^{2+} ions. It was found that, to obtain an optical attenuation close to the one corresponding to 0.5 Gy, we had to store the FXG gel flasks at room temperature (20 – 22 °C) for at least 8 h prior to irradiation. Therefore, the linear FXG gel response is extended on the 0 – 4 Gy dose range, allowing to measure even the smallest out-of-field doses in a treatment plan.

Consequently, 3D measurements on the 0 – 10 Gy dose range can be performed with optical CT readings of FXG gel dosimeters at wavelengths 590 nm and 633 nm. Small-field dose profile measurements (2 x 2 cm^2 6 MV WFF and 1 x 1 cm^2 6 MV FFF dose profiles) were conducted with FXG gel dosimeters and a microDiamond detector (PTW). The γ-index analysis (0.5%/0.5mm) gave a γ passing rate of 93.4 %, displaying a very close agreement between the two dosimeters and validating the dual wavelength reading method of FXG gels we implemented in our lab.

A next step of optimization of the dual wavelength reading method is under development at our lab. Instead of using two different light sources emitting at 590 nm and 633 nm, it is planned to use a white light source and to switch easily the bandpass filter (of wavelength 590 nm or 633 nm) in front of it. This way, the optical readout will be more user-friendly, the readings will be faster and there will be no need to constantly heat the light sources with an external power supply for thermal stabilization. It will then be possible to study the feasibility of implementing a 3D end-to-end quality assurance in stereotactic or dynamic radiotherapy with FXG gel dosimeters and the dual wavelength reading method presented here.

5. Conclusion

This study presents the optimization of a FXG gel composition and the development of a new dual wavelength reading method by optical CT scanner for widening the dose range of use of FXG gel dosimeters for 3D stereotactic applications, e.g. by measuring doses higher than 4 Gy.

This reading method was developed on the Vista16™ scanner by combining low dose values (< 4 Gy) read at 590 nm to high dose values (between 4 Gy and 10 Gy) read at 633 nm. The overall dosimetric method has the ability to provide a linear dose response up to 10 Gy, with the best achievable sensitivity, and without dose rate or energy dependency observed in the limits of the uncertainties in the ranges of interest.

Comparison of small-field profile measurements performed with FXG gel and microDiamond detectors displayed a γ-index passing rate of 93.4 % for strict passing criteria 0.5%/0.5mm, validating the use of this dual wavelength reading method. A feasibility study, with an actual treatment plan, must now be performed to implement a 3D end-to-end quality assurance with this new dosimetric method in stereotactic radiotherapy.

Acknowledgments:
We thank Jennifer Dietrich of ModusQA for her help with the Vista16™ optical CT scanner, and Marion Baumann and Julien Jurczak for the small-field profile measurements with the microDiamond detector.

Funding sources:
This research was supported by the French metrology institute (Laboratoire National de métrologie et d'essais, LNE) and by the CEA (Commissariat à l'Energie Atomique et aux énergies alternatives).

Figure captions:

Fig. 1: (a) PMMA cuvettes and (b) Teflon-FEP cylinders filled with FXG gel and exposed to absorbed doses up to 16 Gy.

Fig. 2: Schematic representation of the ferric ion diffusion experiment (based on Coulaud *et al* 2019 [15]).

Fig. 3: (a) Dose response curves up to 14 Gy for different pH values between 0.5 and 3.5. The rest of the gel composition is 5 %wt gelatin, 0.3 mM ferrous ammonium sulfate and 0.04 mM XO. Error bars are smaller than the symbol size. (b) Linear regressions on the 1 – 6 Gy dose range for pH values 1.56, 1.70 and 1.85.

Fig. 4: (a) Dose response curves on the 2 – 22 Gy dose range for XO concentrations between 0.04 mM and 0.13 mM. The rest of the gel composition is 5 %wt gelatin, a pH of 1.6 and 0.3 mM ferrous ammonium sulfate. Error bars are smaller than the symbol size. (b) Sensitivity of linear gel dose response (black triangles) and maximal dose until which the gel dose response is linear for a given XO concentration (orange circles).

Fig. 5: (a) Dose response curves for ferrous ammonium sulfate concentrations between 0.3 mM and 0.6 mM on the 2 – 20 Gy dose range. The rest of the gel composition is 5 %wt gelatin, a pH of 1.6 and 0.11 mM XO. Error bars are smaller than the symbol size. (b) Sensitivity of dose response curves with Fe^{2+} ion concentration.

Fig. 6: Absorbance spectra of the FXG gel exposed to doses up to 10 Gy. The FXG gel composition is 5 %wt gelatin, a pH of 1.6, 0.3 mM ferrous ammonium sulfate and 0.09 mM XO. The XO-Fe(III) complex absorption peak is visible around 585 nm. The FXG gel dose responses at wavelengths 590 nm and 633 nm are highlighted as they correspond to the reading wavelengths on the optical CT scanner.

Fig. 7: Optical attenuation coefficients measured repeatedly for two hours of cuvettes exposed to 2 Gy, 5 Gy and 10 Gy. Error bars are smaller than the symbol size.

Fig. 8: (a) Optical attenuation profiles of a gel dosimeter irradiated on one half at 5 Gy. The three profiles come from projections acquired at 44 min, 193 min and 381 min after irradiation. (b) Variation of $\sigma^2/2$ with time after irradiation.

Fig. 9: Polynomial gel dose response (a) on the 0.25 – 5 Gy dose range for the optical CT reading at 590 nm and (b) on the 0.25 – 10 Gy dose range for the optical CT reading at 633 nm. Dose resolution (black circles) and relative dose resolution (red triangles) at 590 nm (c) and 633 nm (d). The dotted lines in the four graphs delimit the absorbed dose range where the gel response is linear.

Fig. 10: FXG gel dose response for low doses between 0.05 Gy and 3 Gy measured at 590 nm. Two linear regimes were found and are separate at the 0.5 Gy dose value. The inset displays the response in the 0.05 – 0.5 Gy dose range.

Fig. 11: (a) Dependence of gel dosimeter sensitivity for 10 cuvettes exposed to 5 Gy at different dose rates for a 6 MV WFF photon beam. (b) Dependence of gel dosimeter sensitivity on quality index ($TPR_{20,10}$) for cuvettes exposed to 5 Gy at photon energies 6, 10, 15 and 20 MV WFF (400 MU/min dose rate).

Fig. 12: Absorbed dose profiles of two gel dosimeters exposed to (a) a 8.9 Gy 2 x 2 cm^2 6 MV WFF irradiation and (c) a 8.6 Gy 1 x 1 cm^2 6 MV FFF irradiation, and scanned at wavelengths 590 nm and 633 nm. (b), (d): Gel and microDiamond relative dose profiles of the same irradiation field with a γ-analysis of passing criteria 0.5%/0.5mm (green and red stars). The black line represents $\gamma = 1$.

Gel components	Gelatin concentration (%wt)	pH	Ferrous ammonium sulfate concentration (mM)	Xylenol orange concentration (mM)	Number of batches
Experiment 1	5	**0.5 – 3.5**	0.3	0.04	10
Experiment 2	**4 – 6**	1.6	0.3	0.04	3
Experiment 3	5	1.6	0.3	**0.04 – 0.13**	7
Experiment 4	5	1.6	**0.3 – 0.6**	0.11	4

Table 1: Concentrations of the components of the FXG gel and its pH in the experiments performed to find the optimal FXG gel composition for stereotactic and dynamic treatment 3D QA. The number of FXG gel batches used for each experiment can be found in the last column.

Source of uncertainty	Type A	Type B
Repositioning of the flask	$3.7\ 10^{-3}$ cm^{-1}	
Spontaneous oxidation correction	Std dev in a ROI (r=5 mm, h=10 mm) at the center of an unirradiated gel flask	
Reading temperature variation		$1.1\ 10^{-3}$ cm^{-1}
Post-irradiation waiting time t_{wait}		$\frac{0.01}{2\sqrt{3}} * \Delta\mu$ if 20 min $\leq t_{wait} \leq 50$ min
Diffusion effects		Negligible if $t_{wait} < 50$ min
Calibration flasks	Std dev in a ROI (r=5 mm, h=10 mm) at the center of the calibration flask	
Inter-batch reproducibility	Not considered if calibration flasks and flasks used for the measurements are from the same batch	
Intra-batch reproducibility	Included if number of calibration flasks ≥ 8	

Table 2: Uncertainty budget (k=1) for the optical attenuation coefficients $\Delta\mu$ measured in the calibration flasks and the flasks used for the profile measurements (std dev = standard deviation, r = radius and h = height).

Gelatin concentration (%wt)	Sensitivity (cm^{-1} Gy^{-1})	Initial absorbance
4	0.172 ± 0.013	0.147 ± 0.001
5	0.169 ± 0.013	0.164 ± 0.001
6	0.167 ± 0.007	0.167 ± 0.001

Table 3: Sensitivities on the absorbed dose range up to 6 Gy and initial absorbance values for gelatin concentrations of 4 %wt, 5 %wt and 6 %wt. The rest of the gel composition is a pH of 1.6, 0.3 mM ferrous ammonium sulfate and 0.04 mM XO.

Wavelength reading (nm)	$D_{\Delta}^{95\%}$ (Gy)	$D_{\Delta,\%}^{95\%}$ (%)	Absorbed dose range (Gy)
590	0.056 – 0.077	3.8 – 5.6	1 – 2
633	0.32 – 0.43	4.3 – 5.4	6 – 10

Table 4: Best dose resolutions, best relative dose resolutions and their corresponding absorbed dose range for the 590 nm and 633 nm readings.

Field size	2 x 2 cm^2		1 x 1 cm^2	
Detector type	microDiamond	FXG gel	microDiamond	FXG gel
FWHM (mm)	19.6	19.8	9.7	9.9
80%-20% (mm)	3.6	4.1	2.9	3.3
γ passing rate (%)	93.4		93.4	

Table 5: FWHM, 80%-20% penumbra widths and γ passing rates (0.5%/0.5mm) for microDiamond and FXG gel dosimeters.

Gel composition and concentrations in mM	Temperature	d (10^{-10} m^2 s^{-1})	Reference
g5, pH=1.6, Fe^{2+} 0.3, XO 0.09	22 °C	2.46 ± 0.04	This study
g5, S25, Fe^{2+} 0.5, XO 0.1	24 °C	2.03 ± 0.08	Solc *et* Spevacek 2009 [21]
g5, S25, Fe^{2+} 0.5, XO 0.1	23°C	2.22 ± 0.01	Oliveira *et al* 2014 [22]

Table 6: Ferric ion diffusion coefficients of FXG gel dosimeters reported in the literature (g=gelatin, S=sulfuric acid, XO=xylenol orange) for similar gel compositions.

Gel type	Reading method	$D_{\Delta}^{95\%}$ (Gy)	Absorbed dose (Gy)	Reference
Fricke-based with XO	Optical CT at 567 nm (maximum absorption peak ≈ 560 nm)	0.2	0 – 3	Viti *et al* 2006 [23]
Polymer (PAGAT)	MRI	≈ 0.3 – 0.46	0 – 10	Vandecasteele *et* De Deene 2013 [24]
Fricke-based	MRI	0.87	5	Cho *et al* 2013 [25]

Table 7: Dose resolutions for different types of dosimetric gel and reading methods in the literature.

References:

[1] Kozicki M, Berg A, Maras P, Jaszczak M, Dudek M. Clinical radiotherapy application of N-vinylpyrrolidone-containing 3D polymer gel dosimeters with remote external MR-reading. Phys Med 2020;69:134–46. https://doi.org/10.1016/j.ejmp.2019.11.014.

[2] Matrosic CK, Culberson W, Shepard A, Jupitz S, Bednarz B. 3D dosimetric validation of ultrasound-guided radiotherapy with a dynamically deformable abdominal phantom. Phys Med 2021;84:159–67. https://doi.org/10.1016/j.ejmp.2021.04.007.

[3] Babic S, Battista J, Jordan K. Three-Dimensional Dose Verification for Intensity-Modulated Radiation Therapy in the Radiological Physics Centre Head-and-Neck Phantom Using Optical Computed Tomography Scans of Ferrous Xylenol–Orange Gel Dosimeters. Int J Radiat Oncol 2008;70:1281–91. https://doi.org/10.1016/j.ijrobp.2007.11.032.

[4] Schreiner LJ. True 3D chemical dosimetry (gels, plastics): Development and clinical role. J Phys Conf Ser 2015;573:012003. https://doi.org/10.1088/1742-6596/573/1/012003.

[5] Gore JC, Kang YS, Schulz RJ. Measurement of radiation dose distributions by nuclear magnetic resonance (NMR) imaging. Phys Med Biol 1984;29:1189–97. https://doi.org/10.1088/0031-9155/29/10/002.

[6] Schreiner LJ. Review of Fricke gel dosimeters. J Phys Conf Ser 2004;3:9–21. https://doi.org/10.1088/1742-6596/3/1/003.

[7] Kron T, Jonas D, Pope JM. Fast T1 imaging of dual gel samples for diffusion measurements in NMR dosimetry gels. Magn Reson Imaging 1997;15:211–21. https://doi.org/10.1016/S0730-725X(96)00352-9.

[8] Kelly RG, Jordan KJ, Battista JJ. Optical CT reconstruction of 3D dose distributions using the ferrous-benzoic-xylenol (FBX) gel dosimeter. Med Phys 1998;25:1741–50. https://doi.org/10.1118/1.598356.

[9] Bero MA, Gilboy WB, Glover PM, El-masri HM. Tissue-equivalent gel for non-invasive spatial radiation dose measurements. Nucl Instrum Methods Phys Res Sect B Beam Interact Mater At 2000;166–167:820–5. https://doi.org/10.1016/S0168-583X(99)00873-3.

[10] Del Lama LS, Petchevist PCD, de Almeida A. Fricke Xylenol Gel characterization at megavoltage radiation energy. Nucl Instrum Methods Phys Res Sect B Beam Interact Mater At 2017;394:89–96. https://doi.org/10.1016/j.nimb.2016.12.045.

[11] Davies JB, Baldock C. Sensitivity and stability of the Fricke–gelatin–xylenol orange gel dosimeter. Radiat Phys Chem 2008;77:690–6. https://doi.org/10.1016/j.radphyschem.2008.01.007.

[12] Ramm D. A fast dual wavelength laser beam fluid-less optical CT scanner for radiotherapy 3D gel dosimetry II: dosimetric performance. Phys Med Biol 2018;63:045020. https://doi.org/10.1088/1361-6560/aaaa46.

[13] Dekker KH, Hazarika R, Jordan KJ. Stray light in cone beam optical computed tomography: III. Evaluation of a redesigned large-volume commercial scanner based on a convergent light source. Phys Med Biol 2018;63:21NT02. https://doi.org/10.1088/1361-6560/aae79d.

[14] Olding T, Schreiner LJ. Cone-beam optical computed tomography for gel dosimetry II: imaging protocols. Phys Med Biol 2011;56:1259–79. https://doi.org/10.1088/0031-9155/56/5/003.

[15] Coulaud J, Stien C, Gonneau E, Fiallo M, Brumas V, Sharrock P. A new spectroscopic method for measuring ferric diffusion coefficient in gelatin-based dosimeter gels. Biomed Phys Eng Express 2019;5:065028. https://doi.org/10.1088/2057-1976/ab50ce.

[16] Baldock C, Lepage M, Back SÅJ, Murry PJ, Jayasekera PM, Porter D, et al. Dose resolution in radiotherapy polymer gel dosimetry: effect of echo spacing in MRI pulse sequence. Phys Med Biol 2001;46:449–60. https://doi.org/10.1088/0031-9155/46/2/312.

[17] Trapp JV, Michael G, Evans PM, Baldock C, Leach MO, Webb S. Dose resolution in gel dosimetry: effect of uncertainty in the calibration function. Phys Med Biol 2004;49:N139–46. https://doi.org/10.1088/0031-9155/49/10/N02.

[18] Saur S, Strickert T, Wasboe E, Frengen J. Fricke gel as a tool for dose distribution verification: optimization and characterization. Phys Med Biol 2005;50:5251–61. https://doi.org/10.1088/0031-9155/50/22/003.
[19] Babic S, Battista J, Jordan K. An apparent threshold dose response in ferrous xylenol-orange gel dosimeters when scanned with a yellow light source. Phys Med Biol 2008;53:1637–50. https://doi.org/10.1088/0031-9155/53/6/009.
[20] Hussein M, Clark CH, Nisbet A. Challenges in calculation of the gamma index in radiotherapy – Towards good practice. Phys Med 2017;36:1–11. https://doi.org/10.1016/j.ejmp.2017.03.001.
[21] Solc J, Spevacek V. New radiochromic gel for 3D dosimetry based on Turnbull blue: basic properties. Phys Med Biol 2009;54:5095–107. https://doi.org/10.1088/0031-9155/54/17/002.
[22] Oliveira LN de, Sampaio FGA, Moreira MV, Almeida A de. Measurements of the Fe3+ diffusion coefficient in Fricke Xylenol gel using optical density measurements. Appl Radiat Isot 2014;90:241-44. https://doi.org/10.1016/j.apradiso.2014.04.004.
[23] Viti V, d'Errico F, Pacilio M, Luciani AM, Palma A, Grande S, et al. Optical imaging of dose distributions in Fricke gels. Radiat Prot Dosimetry 2006;120:148–50. https://doi.org/10.1093/rpd/ncj005.
[24] Vandecasteele J, De Deene Y. On the validity of 3D polymer gel dosimetry: I. Reproducibility study. Phys Med Biol 2013;58:19–42. https://doi.org/10.1088/0031-9155/58/1/19.
[25] Cho N-Y, Huang S-C, Chung W-Y, Guo W-Y, Chu W-C. Isotropic three-dimensional MRI-Fricke-infused gel dosimetry. Med Phys 2013;40:052101. https://doi.org/10.1118/1.4798228.

Figure 1

Click here to access/download;Figure;FIG1.pptx

Figure 2

Click here to access/download;Figure;FIG2.pptx

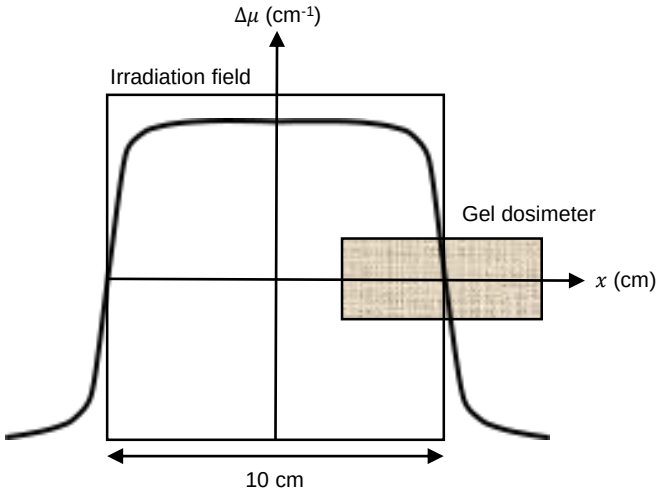

Figure 3

Click here to access/download;Figure;FIG3.pptx

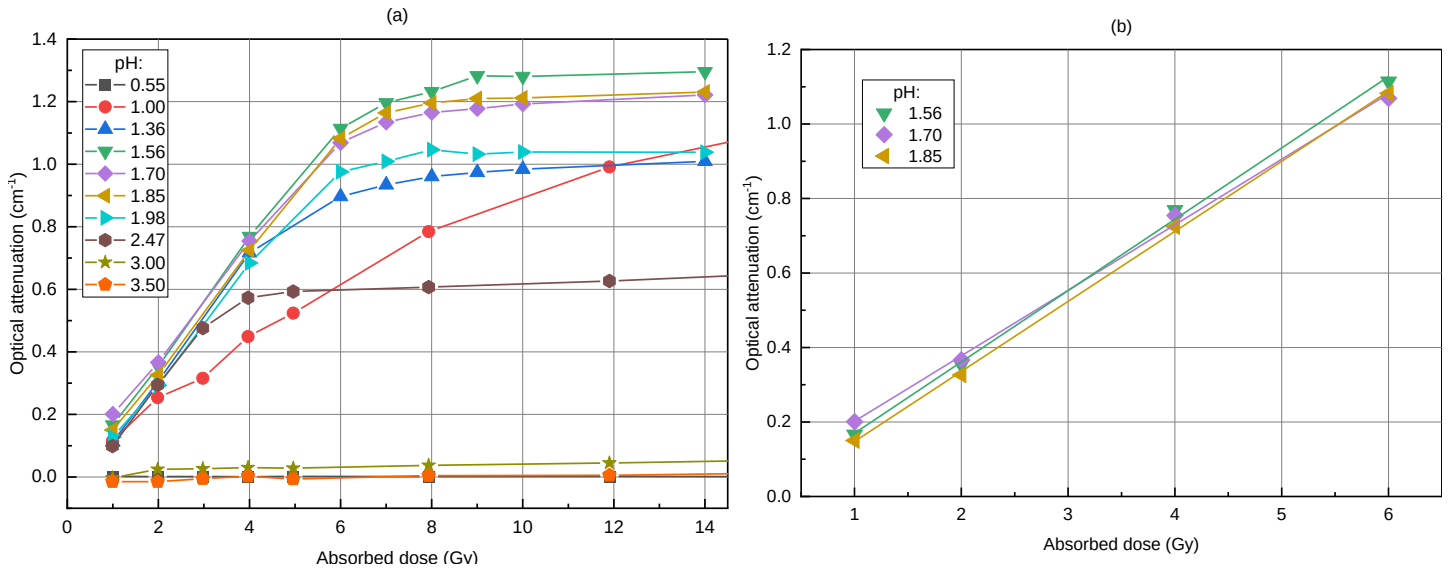

Figure 4

Click here to access/download;Figure;FIG4.pptx

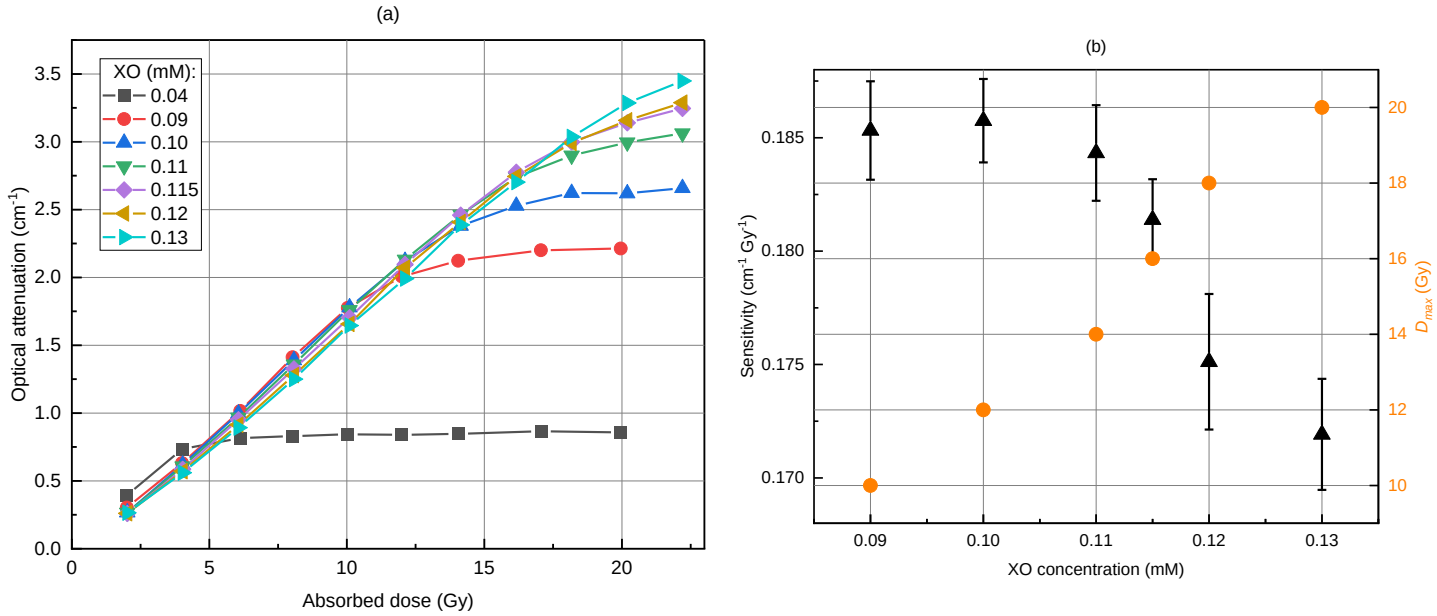

Figure 5

Click here to access/download;Figure;FIG5.pptx

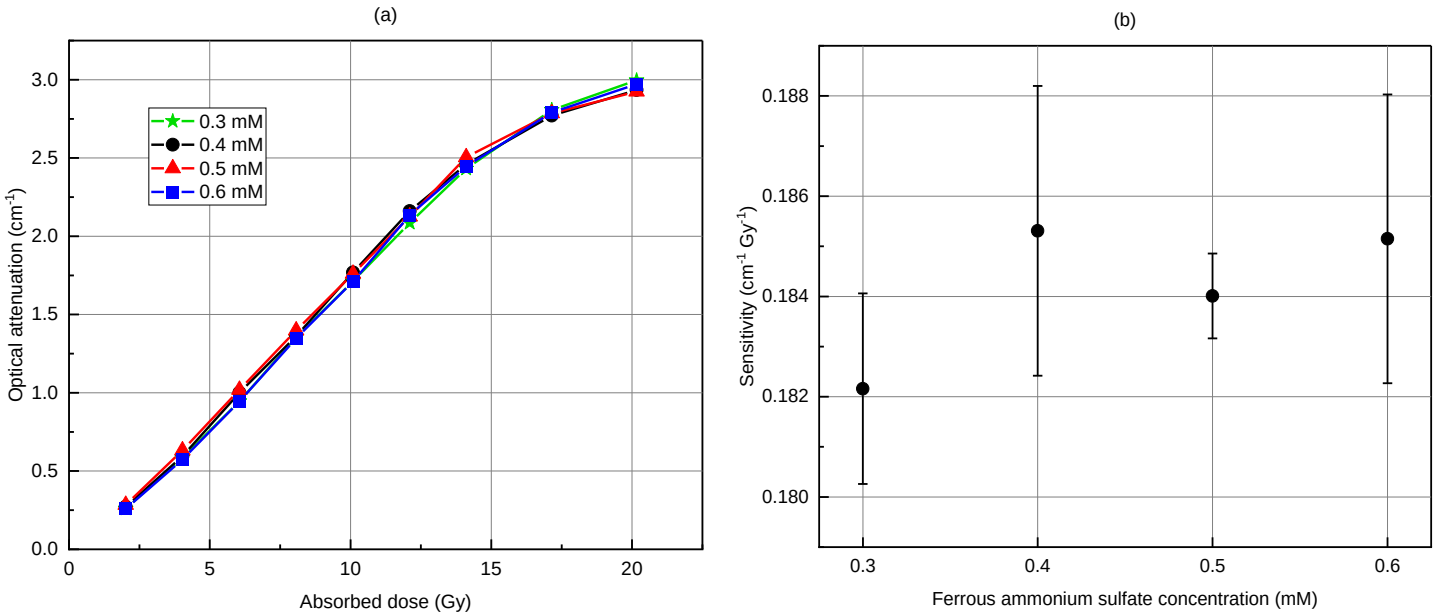

Figure 6

Click here to access/download;Figure

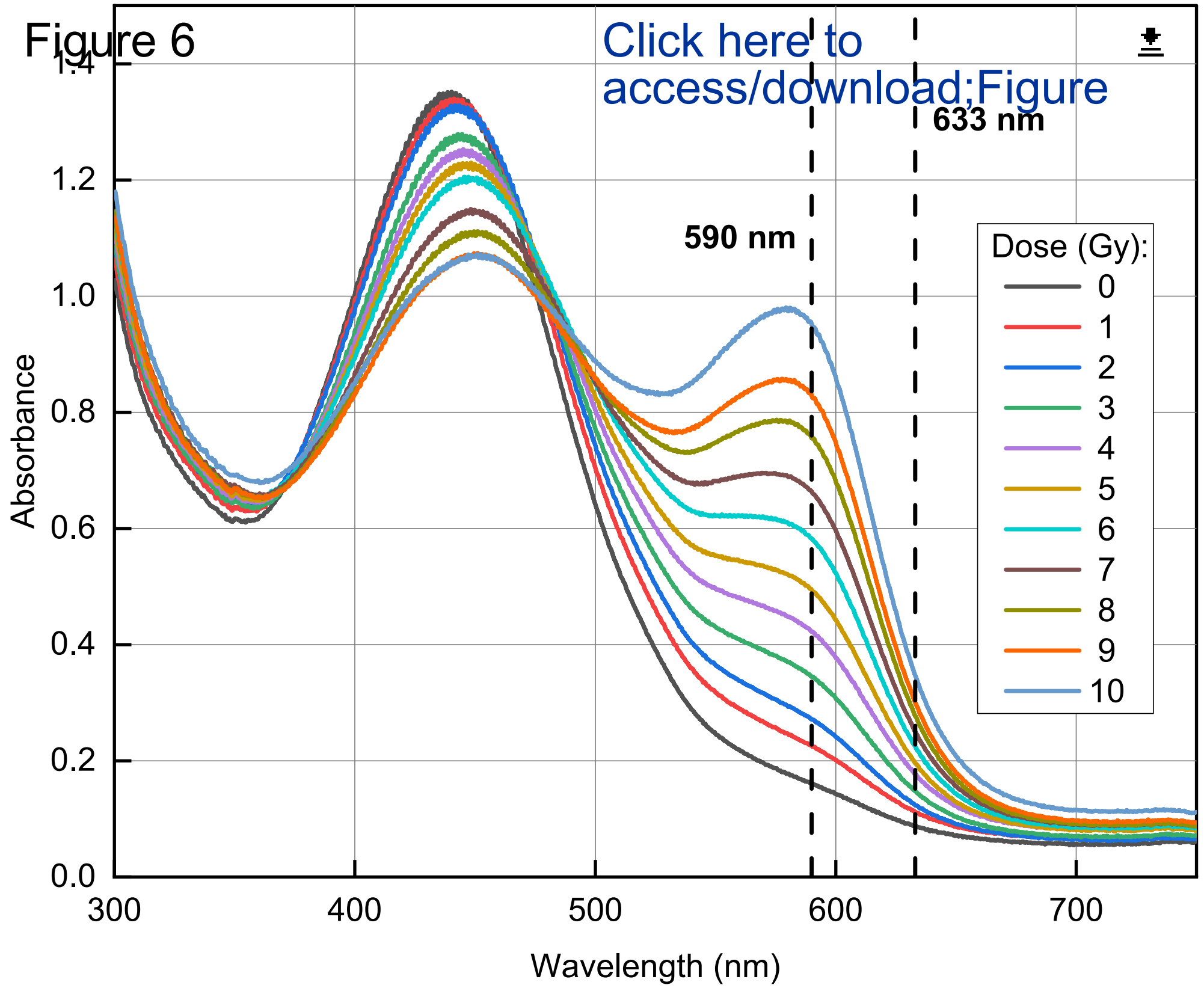

Figure 7

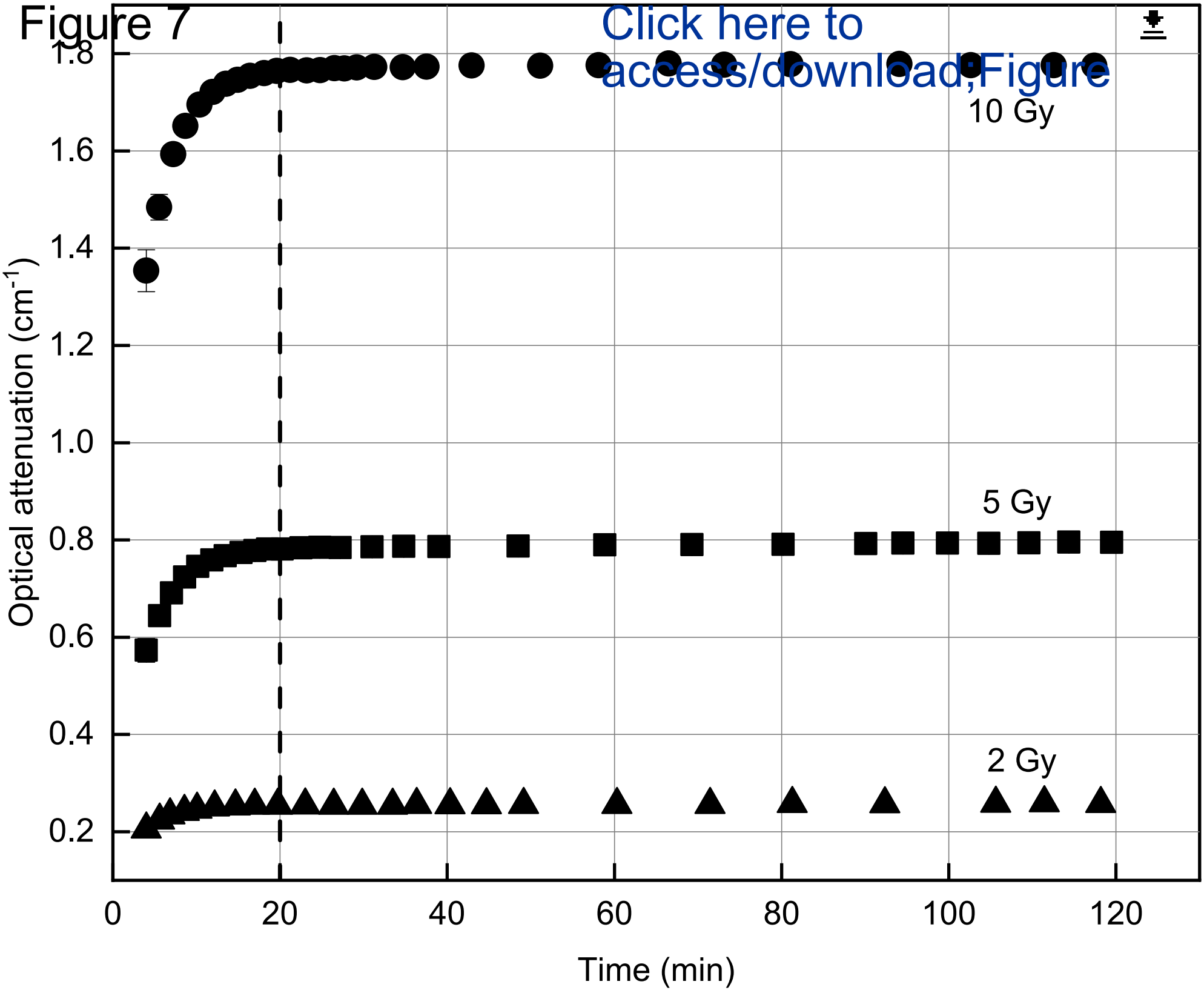

Figure 8

Click here to access/download;Figure;FIG8.pptx

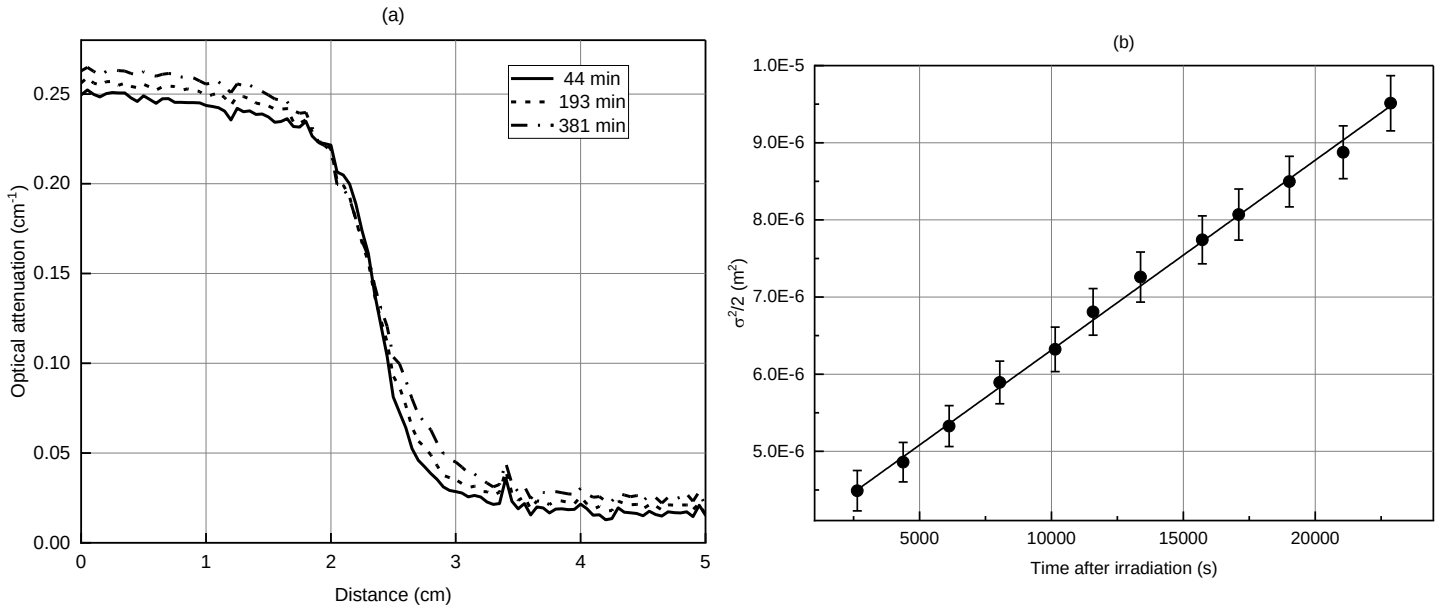

Figure 9

Click here to access/download;Figure;FIG9.pptx

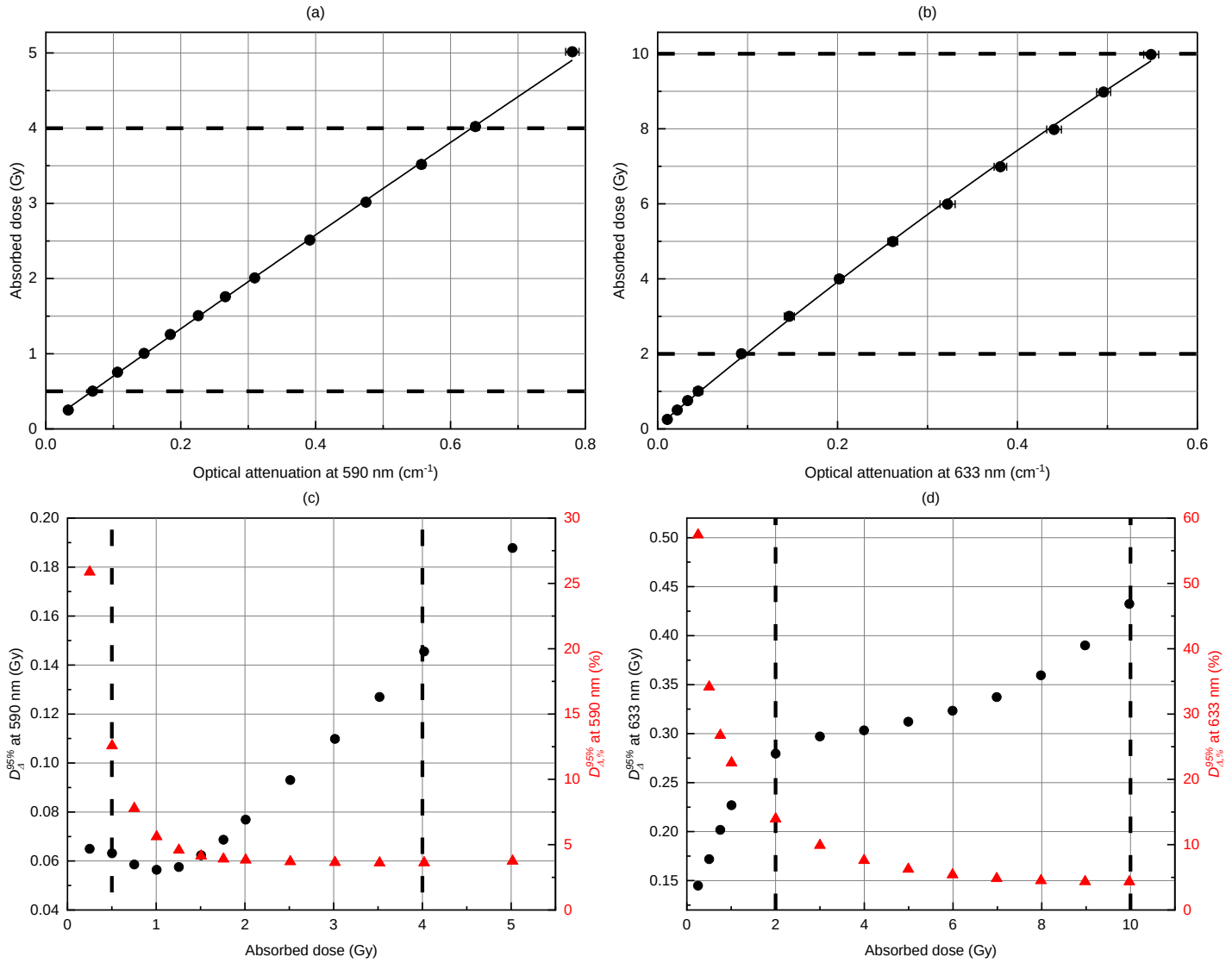

Figure 10

Click here to access/download;Figure;FIG10.pptx

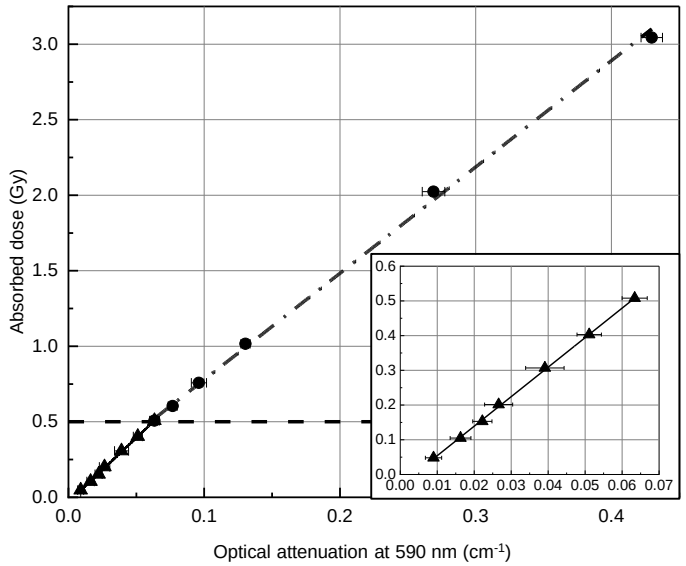

Figure 11

Click here to access/download;Figure;FIG11.pptx

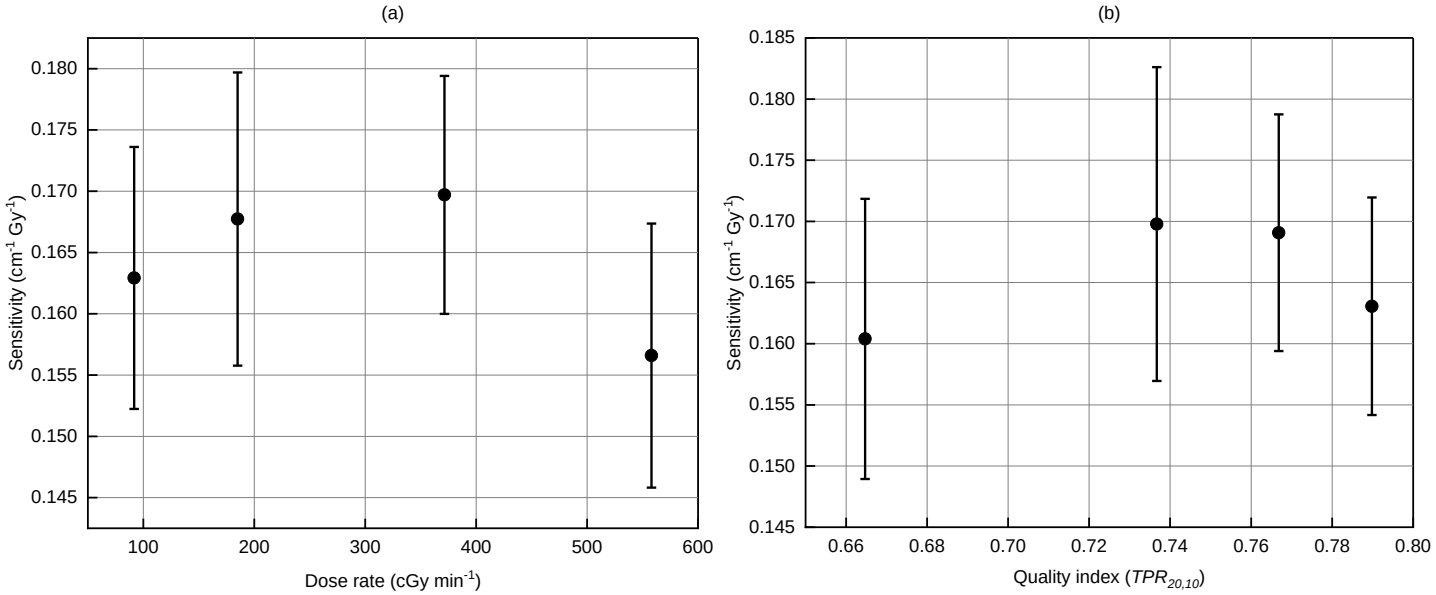

Figure 12

Click here to access/download;Figure;FIG12.pptx